minerals

MDPI

Article

Reducing Media of the Zhiluo Formation in the Saitai Area, Ordos Basin, and Their Roles in Uranium Mineralization

Qinghong Si [1,2,3,4,*], Deqiang Tian [5,6,*], Zhaojian Wu [5], Yaqi Huang [2,4], Chao Zhang [2,4], Xiaoyu Guo [7], Wei Guo [8], Hongwei Deng [8] and Jiapeng Tian [7]

1 School of Resources and Environmental Engineering, Hefei University of Technology, Hefei 230002, China
2 Tianjin Center, China Geological Survey (North China Center of Geoscience Innovation), Tianjin 300170, China; hyaq_1014@163.com (Y.H.); quickzc@sina.com (C.Z.)
3 Institute of Geomechanics, Chinese Academy of Geological Sciences, Beijing 100081, China
4 Key Laboratory of Uranium Geology of China Geological Survey, Tianjin 300170, China
5 CGNPC Uranium Resources Co., Ltd., Beijing 100048, China; wuzhj06@126.com
6 College of Earth and Environmental Sciences, Lanzhou University, Lanzhou 730000, China
7 Inner Mongolia Coal Construction Engineering (Group) Corporation, Hohhot 010010, China; 13474706661@139.com (X.G.); xiaofei158866@163.com (J.T.)
8 School of Resources, Environment and Jewelry, Jiangxi College of Applied Technology, Ganzhou 341000, China; 15350362134@163.com (W.G.); 18172892906@163.com (H.D.)
* Correspondence: sqinghongcgs@163.com (Q.S.); tiandeqiang@163.com (D.T.)

Abstract

Uranium mineralization in the Zhiluo Formation of the Saitai area preferentially occurs in carbonaceous debris- and pyrite-rich sandstones. This study characterizes ore fluid and reducing medium controls on uranium enrichment and uranium mineral genesis using core observations, SEM, EPMA, and geochemical tests. Uranium minerals mainly form zoned aggregates around carbonaceous debris, occur with colloform pyrite within feldspar and carbonate dissolution pores, and appear within zones of biotite breakdown. Whole-rock geochemical data from ore-bearing sandstone show variations: U(IV)/U(VI) (0.625–34.78; corresponding to U(IV)/total U of 0.38–0.97), Ce/Ce* (0.72–1.01), Fe^{2+}/Fe^{3+} (0.70–92.35; Fe^{2+}/total Fe of 0.41–0.99), TOC (0.026–3.35%), total sulfur (0.1–0.3%), and S^{2-} (3.4×10^{-6}–83.3×10^{-6}). Fluid inclusions in calcite cements show homogenization temperatures of 130–183 °C, and those hosted in intergranular calcite cluster at 130–138 °C, with salinities of 0.9–9.5 wt.% NaCl equivalent and CO_2-bearing characteristics. Mineralization of the Zhiluo Formation developed in a medium–low temperature, reducing alkaline environment. Carbonaceous debris shows close spatial and genetic links with uranium minerals. Authigenic pyrite correlates with uranium through paragenetic association with carbonaceous fragments. Alkaline fluid dissolution provides pore space for uranium and secondary pyrite precipitation.

Keywords: Zhiluo Formation; Saitai area; Ordos Basin; reducing media; ore-forming fluids; uranium mineralization

Check for updates

Academic Editor: Sergey V. Krivovichev

Received: 26 August 2026
Revised: 28 September 2026
Accepted: 29 September 2026
Published: 3 October 2026

Copyright: © 2026 by the authors. Licensee MDPI, Basel, Switzerland. This article is an open access article distributed under the terms and conditions of the Creative Commons Attribution (CC BY) license.

1. Introduction

A series of uranium deposits and mineral occurrences (Daying, Nalinggou, Zaohuohao, Bayinqinggeli, and Tarangaole [1–5]) were successively discovered in the northern Ordos Basin. New uranium mineralization was also found in peripheral areas, such as Saitai [6] and Telaaobao [7,8]. In the Saitai area of the northern Ordos Basin, high-grade uranium mineralization within the Zhiluo Formation commonly occurs in intervals rich in reducing

media such as carbonaceous debris and pyrite [9]. Revealing the characteristics of these reducing media and their roles in uranium metallogenesis is critical for understanding uranium metallogenic theory and establishing exploration criteria.

Globally, sandstone-hosted uranium deposits form through redox interactions between oxidizing uranium-bearing fluids and various reducing substrates, among which organic matter, pyrite, and hydrocarbon fluids are widely recognized as critical reductants controlling uranium precipitation [10–13]. The Ordos Basin has been documented in international uranium deposit monographs as a typical multi-energy resource basin hosting sandstone-type uranium deposits in the Middle Jurassic Zhiluo Formation [14,15]. Previous international investigations in the Ordos Basin have confirmed that basin-derived hydrocarbon fluids participate in regional uranium mineralization [16]. On the basis of this unified global metallogenic framework, this study focuses on the in situ solid reductants within sandstone bodies, mainly carbonaceous debris and fine-grained pyrite, and further clarifies their detailed contributions to local uranium enrichment.

Reducing media are fundamental for the development of sandstone-hosted uranium deposits. It is widely accepted that uranium mobility is governed by its redox state: U(VI) is readily mobile as soluble uranyl complexes, whereas U(IV) is poorly soluble and stable under reducing conditions [11]. Organic matter, pyrite, biotite, and hydrocarbon fluids are the main reducing media of uranium mineralization [17–22]. However, they differ greatly in occurrence, reducing power, and role in ore formation. Organic matter and pyrite are in situ solid reducing media. Widespread organic matter can adsorb uranium ions onto mineral surfaces and reduce soluble U(VI) to insoluble U(IV), resulting in early uranium pre-enrichment [5,11,23]. Pyrite has a stronger reducing ability, so it promotes fast precipitation of uranium minerals [24]. Hydrocarbon fluids are external reducing fluids. These fluids can also overprint prior mineralization to expand the ore bodies and serve as important reductants in oxidizing sedimentary environments where hydrocarbon migration is active and adjacent to oil and gas fields [25–27]. Altered biotite is a weakly reducing medium and may play a role in mineralization locally [28,29].

The Saitai area is a typical "mud-sand-mud" area, and the mineral-bearing sand bodies contain potential reducing media such as pyrite, carbonaceous debris, and biotite [6]. At present, this deposit remains in the exploration phase. However, the spatial relationships between uranium enrichment and reducing media (pyrite and carbonaceous debris) within the Zhiluo Formation sandstones in this region remain poorly constrained. More importantly, the mineralogical attributes of these reductants (morphology, chemical composition), as well as their responses to redox and alkaline fluid conditions, remain poorly understood. This ambiguity in the mineral–environment response relationship directly limits the identification of uranium precipitation processes and enrichment places and hinders a comprehensive understanding of uranium-metallogenic regularities and metallogenic models. Based on the large amount of reducing media present in the uranium-bearing rock series of the Zhiluo Formation, this study investigates petrological–mineralogical characteristics and fluid geochemistry to decipher the mineral–environment response relationship between reducing media and uranium mineralization, and to explore the controlling mechanism of reducing media for uranium enrichment and the corresponding metallogenic model in the Saitai area.

2. Geological Setting

The Saitai area is located in the central part of the Yimeng Uplift in the northern Ordos platform depression (Figure 1b,c). It is located in Inner Mongolia, China. The study area exposes Triassic, Middle Jurassic, Lower Cretaceous, and Quaternary strata (Figure 1d). There is abundant evidence of tectonic movements after the Triassic period

in this area [30,31]. The Indosinian movement at the end of the Triassic led to a parallel unconformity between the Yan'an Formation and the underlying Yanchang Formation [31]. The Yanshan movement produced a parallel disconformity between the Zhiluo Formation and the underlying Yan'an Formation and also caused a low-angle unconformity between the Zhidan Group and the underlying Anding Group [32].

The Middle Jurassic Zhiluo Formation mainly consists of highly permeable braided fluvial sandstones with good connectivity and represents the primary host for sandstone-type uranium deposits [30,31,33]. Underlying this unit is the Yan'an Formation [20], which contains well-developed coal seams and abundant organic reductants, and represents an important target for uranium mineralization within coal-bearing sequences in this area. The strata of the Zhidan Group are gently inclined [31] and show a low angle unconformable contact with the underlying Anding Formation. Jurassic strata mostly exhibit a monocline striking SE and dipping SW. Stratal attitudes show minor variations in strike and dip [34]. There are no faults in Saitai and its structure is simple, and no magmatic rocks have been found.

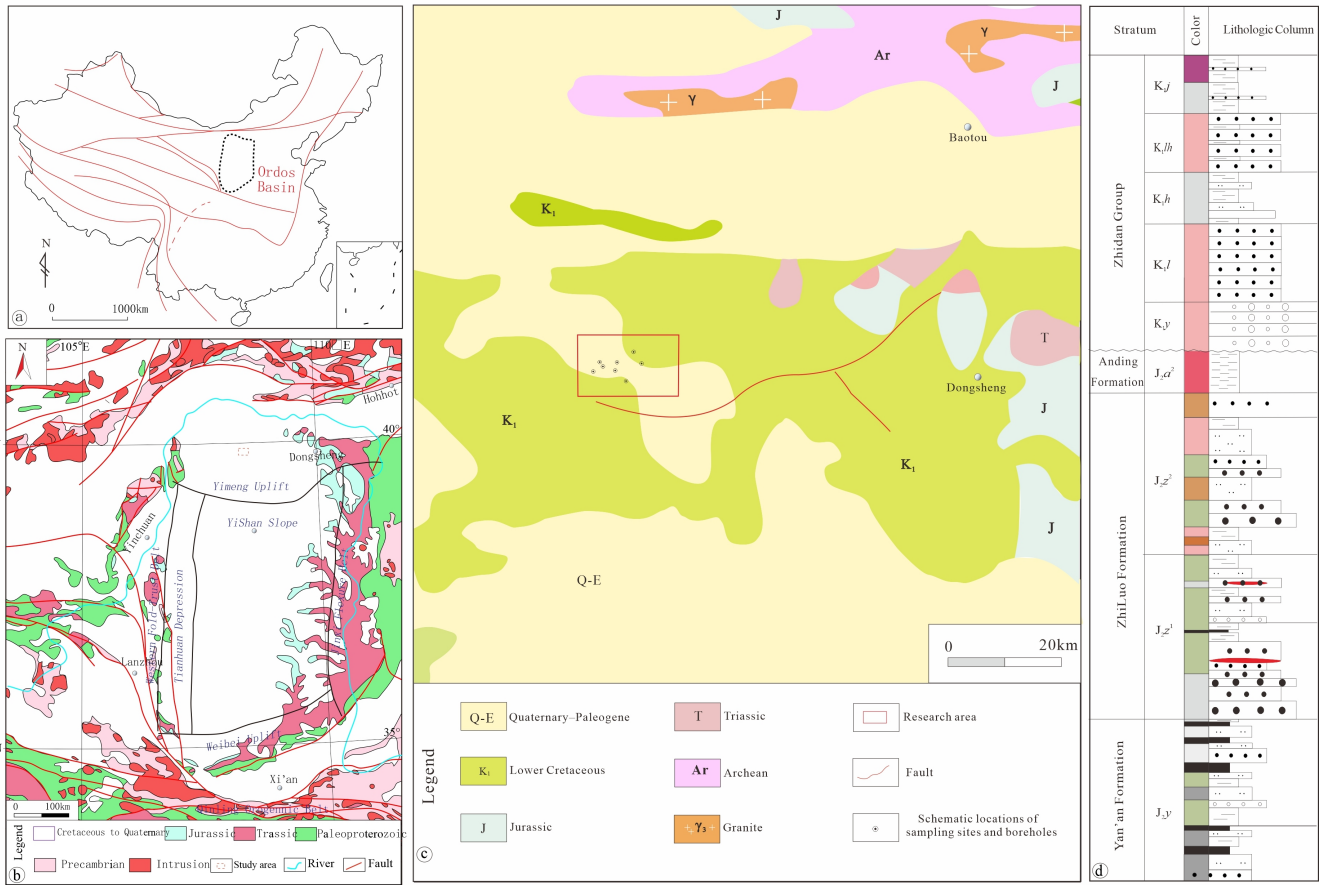


Figure 1. Geological overview and tectonic outline map of the Saitai area in the northern Ordos Basin. (**a**) Location of the Ordos Basin in China; (**b**) Tectonic location of the study area; (**c**) Geological sketch map of the study area; (**d**) Comprehensive lithologic column of the study area. (**a**,**b**) Modified from [35]).

3. Materials and Methods

3.1. Mineralogical Analytical Methods

To understand the relationship between reducing media and uranium mineralization, multi-scale analytical methods were used. Field borehole core logging and polarizing microscope observations were first performed to characterize rock composition, color, strati-

graphic continuity of target sandstones, and the macroscopic occurrence of carbonaceous debris, pyrite, and uranium anomalies. Scanning electron microscopy (SEM) and electron probe microanalyzer (EPMA) analyses were used to characterize microscopic textures and contact relationships between uranium minerals and reduction-altered minerals, including pyrite, chlorite, and ankerite, within ore-bearing sandstone samples. SEM and EPMA analyses were performed at the EPMA Laboratory of Tianjin Center, China Geological Survey, while some partial SEM and energy-dispersive spectroscopy (EDS) analyses were carried out at the Beijing Research Institute of Uranium Geology. EPMA analyses were conducted using a SHIMADZU EPMA-1600 electron probe microanalyzer (SHIMADZU Corporation, Kyoto, Japan) with wavelength-dispersive spectrometry (WDS). For spot analysis, the operating conditions were an accelerating voltage of 15 kV, a beam current of 20nA, and a beam diameter of 5 μm, and the ZAF correction method was adopted. For element mapping analysis, the accelerating voltage was 15 kV, the beam current was 100 nA, and the beam diameter was 1 μm. Identical analytical regions were used for the same group of mapping tests, and each frame corresponded to the scanning signal of each element. Coffinite occurs as fine micron-scale grains (<5 μm) and at low abundance in the studied sandstones, which cannot be readily detected by conventional bulk XRD analysis. Therefore, uranium mineral identification in this study is based on integrated petrographic observation and EPMA microchemical analysis.

3.2. Geochemical Methods and Fluid Inclusion Study

Eight representative boreholes were selected for geochemical sampling and analysis, and the schematic locations of these boreholes are shown in Figure 1c.

A total of 21 sandstone samples were collected from the ore-bearing zone of the Zhiluo Formation in Saitai for major, trace, and rare earth element geochemical analysis. Major-, trace- and rare-earth-element analyses were performed using an iCap RQ+ ICP-MS and a ZXS Primus IV wavelength-dispersive X-ray fluorescence spectrometer at the Tianjin Center, China Geological Survey, Tianjin, China.

A total of 10 samples were collected from the Saitai area to characterize uranium valence speciation. The analytical instrument used was an HD-3025 micro-uranium analyzer. The testing method followed EJ/T 550-2000, "Determination of Uranium in Soil, Rock and Other Samples by Laser-Induced Fluorescence Method". Experiments were conducted at the Beijing Research Institute of Uranium Geology, CNNC.

A total of 82 sandstone samples (ore-bearing sandstones and host rocks) were analyzed for total sulfur and S^{2-}. Among them, valid TOC, Fe^{2+} and Fe^{3+} data were successfully obtained for 60 samples, whereas the remaining samples failed to yield reliable results for these parameters. S^{2-} was measured by the iodometric method (Method 3.3.2 (4), Soil Environmental Monitoring and Analysis Methods, 1st edition) using a microburette. Total sulfur was determined by XRF (ZSX-Primus II; HJ 780-2015, MDL = 0.003%). Fe^{2+} and Fe^{3+} were tested with a 50 mL acid burette following GB/T 14506.14-2010, with supplementary ICP-OES analysis (iCAP6300; JY/T 0567-2020). TOC was determined by titration per DZ/T 0279.27-2016 (MDL = 0.10%) using a 50 mL acid burette. These analyses were carried out at the Analysis and Test Center, No. 203 Research Institute of Nuclear Industry.

Fluid inclusions were examined in representative ore-bearing sandstone samples, with emphasis on fractures in quartz and feldspar and on cements. Microthermometric measurements were carried out at the Beijing Research Institute. A Leica fluorescence microscope was used for these tests. Raman spectroscopic analyses were performed on the vapor bubbles of two-phase aqueous fluid inclusions under microscopic observation, with the laser spot focused precisely on the internal vapor phase. The characteristic CO_2 peaks at ~1285 and 1387 cm^{-1} were considered reliable. A dedicated blank air background spectrum

was not acquired during this analytical session; therefore, the detected N_2 signal was treated only as a qualitative indicator and was not used to reconstruct fluid composition or quantify gas proportions.

4. Results

4.1. Characteristics of Uranium and Associated Minerals

The ore-bearing lithology of the Saitai area is grayish green to gray medium- to coarse-grained sandstone of the Zhiluo Formation. The recovered cores are mostly complete, with much carbonaceous debris and pyrite (Figure 2). Black carbonaceous debris (C) is common throughout the cores. Carbonaceous materials are mostly seen as bed-parallel, discontinuous banded, and patchy aggregates; some carbonaceous laminae show poor lateral continuity, with carbonaceous matter infilling fractures and accumulating as thin carbon-rich layers.

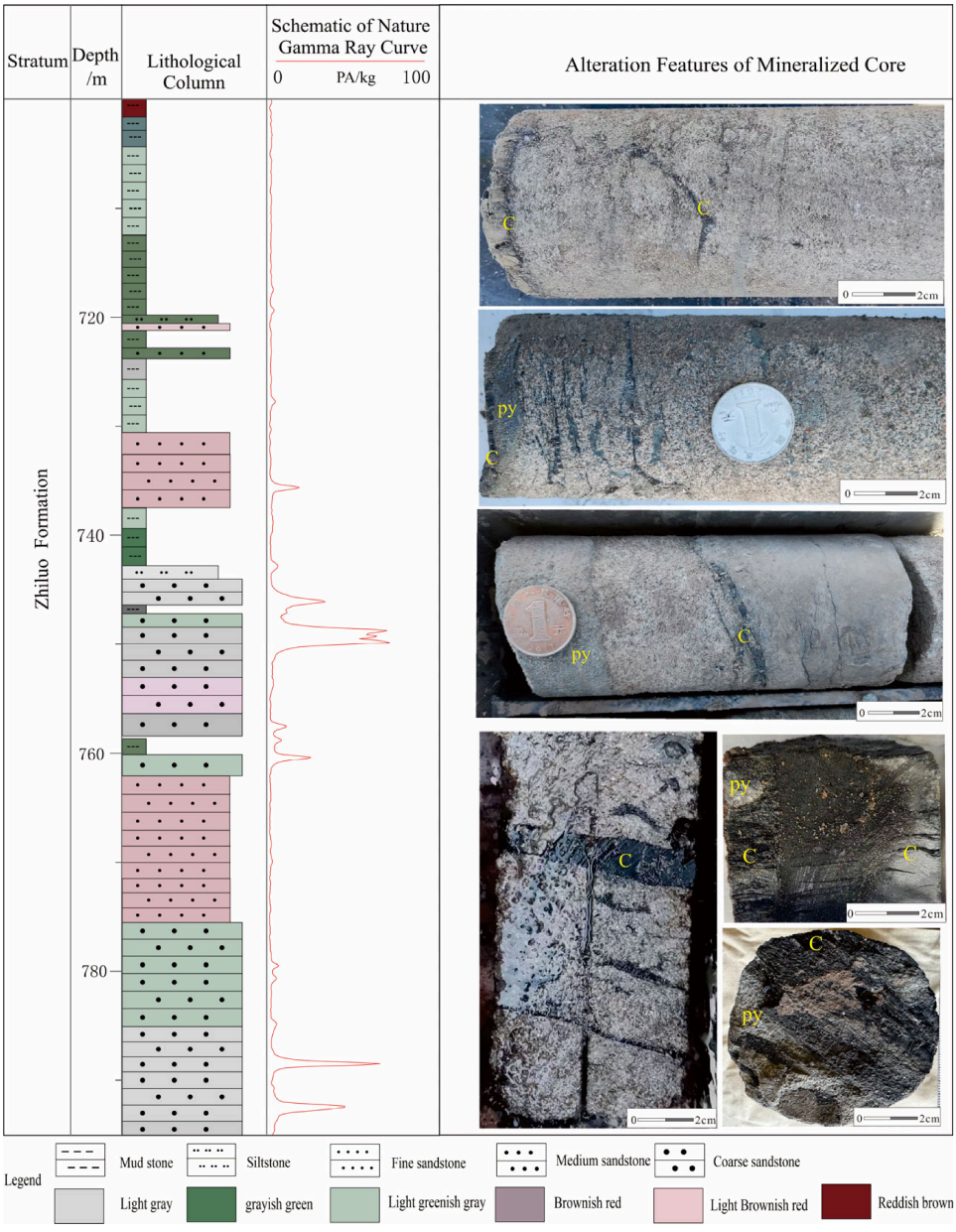


Figure 2. Characteristics of ore-bearing sandstone in the Saitai area, Ordos Basin. Natural gamma-ray log (PSJ-2A instrument, sampling interval 0.05 m); Py—Pyrite; C—Carbonaceous debris.

Pyrite (Py) commonly coexists with carbonaceous components. It occurs as disseminated grains and thin veins within the sandstone matrix, adjacent to carbonaceous debris. Some fractures are filled with carbonaceous matter and pyrite. The pyrite grains in this study show isotropic optical properties under reflected light (no anisotropy or pleochroism) and are therefore identified as pyrite rather than marcasite; the weakly alkaline ore-forming environment also disfavors marcasite precipitation.

Ore-bearing rocks consist of clastic components (~80%), including quartz, feldspar, minor mica fragments, and rock fragments. Quartz content ranges from 45% to 50% and is mostly monocrystalline, with a small amount of siliceous and quartzite fragments. Feldspar accounts for 25–30%, mainly plagioclase and potassium feldspar; plagioclase shows polysynthetic twinning and simple twinning, whereas potassium feldspar exhibits cross-hatched twinning. Rock fragment content is 3–5%, mostly argillaceous rock fragments and altered rock fragments (Figure 3).

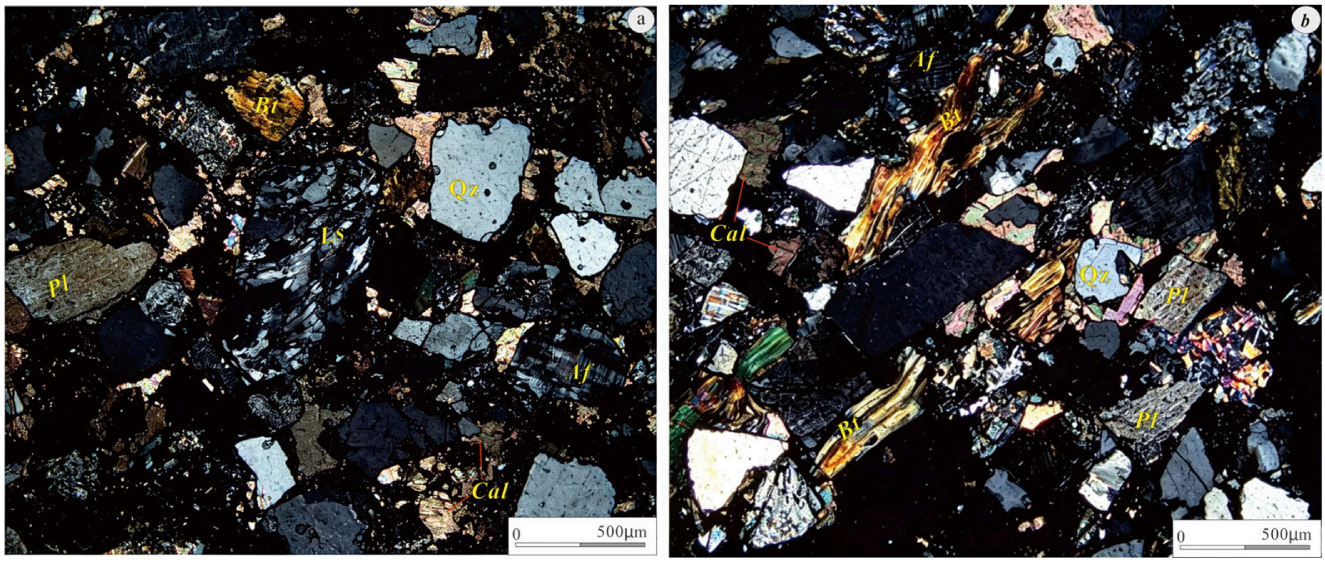


Figure 3. Micrographs of ore-bearing sandstone from the Zhiluo Formation. Qz—Quartz; Pl—Plagioclase; Af—Alkali feldspar; Bt—Biotite; Ls—Siliceous lithic fragments; Cal—Calcite. (**a**) Calcareous medium-grained sandstone; biotite locally bent, moderate compaction; (**b**) Calcareous medium-grained sandstone; biotite aligned, stronger compaction.

The uranium mineralization in the Zhiluo Formation in the Saitai region consists mainly of coffinite. (Figure 4). Neither uraninite nor pitchblende has been identified in the studied samples based on petrographic observation and EPMA analysis. WDS quantitative EPMA spot analyses (Table 1) reveal that coffinite contains consistently high SiO_2 contents (15.46–17.36 wt.%), a diagnostic geochemical signature distinguishing coffinite from pitchblende (which generally has SiO_2 <3 wt.%). BSE observations show that coffinite occurs as discrete bright grains (Figure 4a, spot D1) and as interstitial fillings between detrital clasts (Figure 4b, spot D2).

These minerals occur as irregular granular, dotted, and veinlet forms and are associated with carbonaceous debris, with highly variable grain sizes from several micrometers to hundreds of micrometers and a heterogeneous spatial distribution. Uranium minerals tend to cluster around carbonaceous debris and authigenic pyrite but are seldom observed within authigenic pyrite crystals. Microscopic observations show that uranium minerals form along dissolution fractures within altered biotite, at the edges of dissolved albite, and around carbonaceous debris. They are also closely associated with colloform pyrite within feldspar dissolution vugs and carbonate cements. Bladed chlorite (Chl) is also spatially associated with uranium minerals around biotite and carbonaceous debris (Figure 5).

EPMA backscattered electron (BSE) imaging and elemental maps show the microscopic elemental distributions of the altered feldspar grains. BSE images show the formation of embayed intragranular dissolution pores in feldspar grains, and these pores are filled with high-brightness mineral aggregates. Al and Na are mostly found in the unaltered feldspar domains. Their signals are greatly reduced at the locations of the intragranular dissolution pores. This indicates significant feldspar dissolution. The framework components Al and Na have been mobilized and removed by the fluids. This process generates intragranular secondary pore spaces. These pyrite aggregates occur as clusters within feldspar dissolution pores and have low background values in the fresh feldspar regions, which implies that pyrite aggregates fill the cavities created by feldspar dissolution and are not primary mineral inclusions within the feldspar. The enrichment area of uranium (coffinite) is closely coincident with Fe and S. High uranium signals are confined to feldspar dissolution pores. Neither unaltered feldspar grains nor the surrounding sandstone matrix show obvious uranium enrichment (Figure 6).

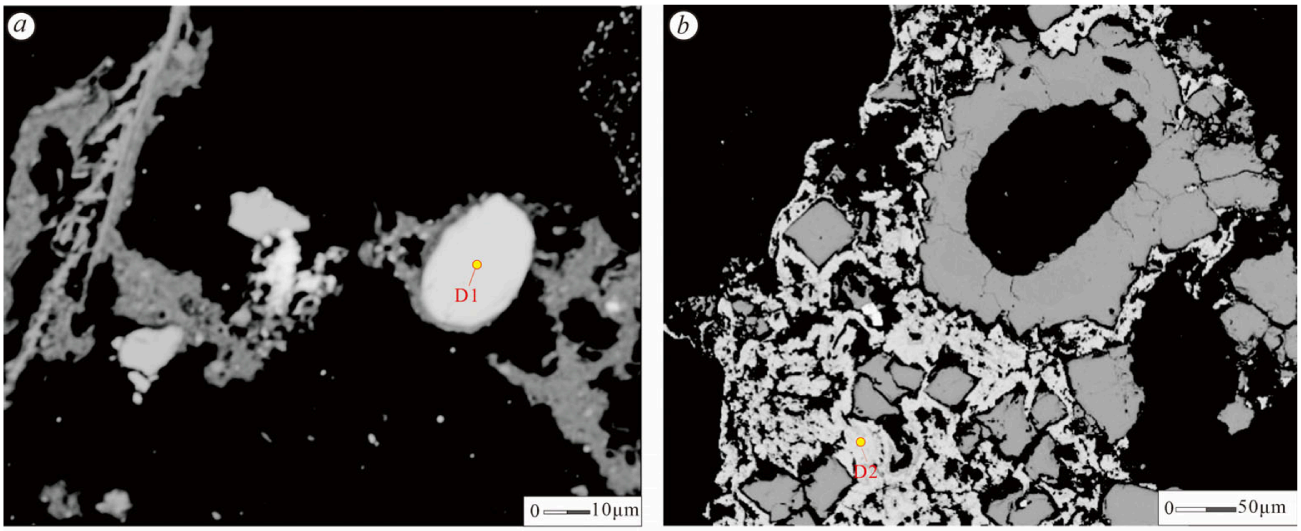


Figure 4. BSE micrographs showing the locations of EPMA analytical spots on coffinite from ore-bearing sandstone of the Zhiluo Formation in the Saitai area. (**a**) Discrete coffinite grain; (**b**) interstitial coffinite filling between detrital clasts.

Table 1. EPMA data of uranium minerals from ore-bearing sandstone samples, Saitai area, Ordos Basin (%).

No.	Na_2O	MgO	Al_2O_3	SiO_2	P_2O_5	SO_3	PbO_2	ThO_2	UO_2	K_2O	CaO	TiO_2	Ce_2O_3	MnO	FeO	Total
D1	0.17	0.02	0.68	17.10	1.05	0.46	0.07	0.00	68.48	0.11	0.35	0.24	1.70	0.00	0.00	90.42
D2	0.30	0.02	0.66	15.79	1.15	1.05	0.22	0.00	76.01	0.07	0.42	0.07	1.60	0.00	1.01	98.36
D3	0.32	0.03	0.61	15.50	1.03	0.86	0.26	0.00	75.92	0.08	0.51	0.13	1.45	0.00	0.35	97.03
D4	0.46	0.04	0.72	16.23	1.09	0.70	0.26	0.00	78.45	0.10	0.51	0.12	1.32	0.00	0.53	100.52
D5	0.26	0.02	0.67	15.66	1.06	0.69	0.18	0.00	78.30	0.10	0.45	0.18	1.45	0.00	0.99	99.99
D6	0.32	0.00	0.68	16.30	1.00	0.63	0.20	0.00	77.38	0.09	0.49	0.12	1.47	0.00	0.41	99.08
D7	0.44	0.04	0.75	17.36	1.15	1.04	0.17	0.00	72.73	0.10	0.42	0.11	1.36	0.00	1.16	96.81
D8	0.39	0.05	0.71	17.05	1.13	1.93	0.12	0.00	72.14	0.09	0.45	0.16	1.40	0.00	1.47	97.09
D9	0.20	0.02	0.63	15.46	1.02	1.53	0.10	0.02	74.68	0.09	0.36	0.05	1.42	0.00	1.78	97.37
D10	0.34	0.03	0.75	16.04	1.05	1.52	0.25	0.04	76.37	0.09	0.44	0.13	1.24	0.00	0.60	98.88
D11	0.36	0.01	0.70	16.09	1.02	1.38	0.20	0.00	75.93	0.09	0.46	0.12	1.43	0.00	0.59	98.37

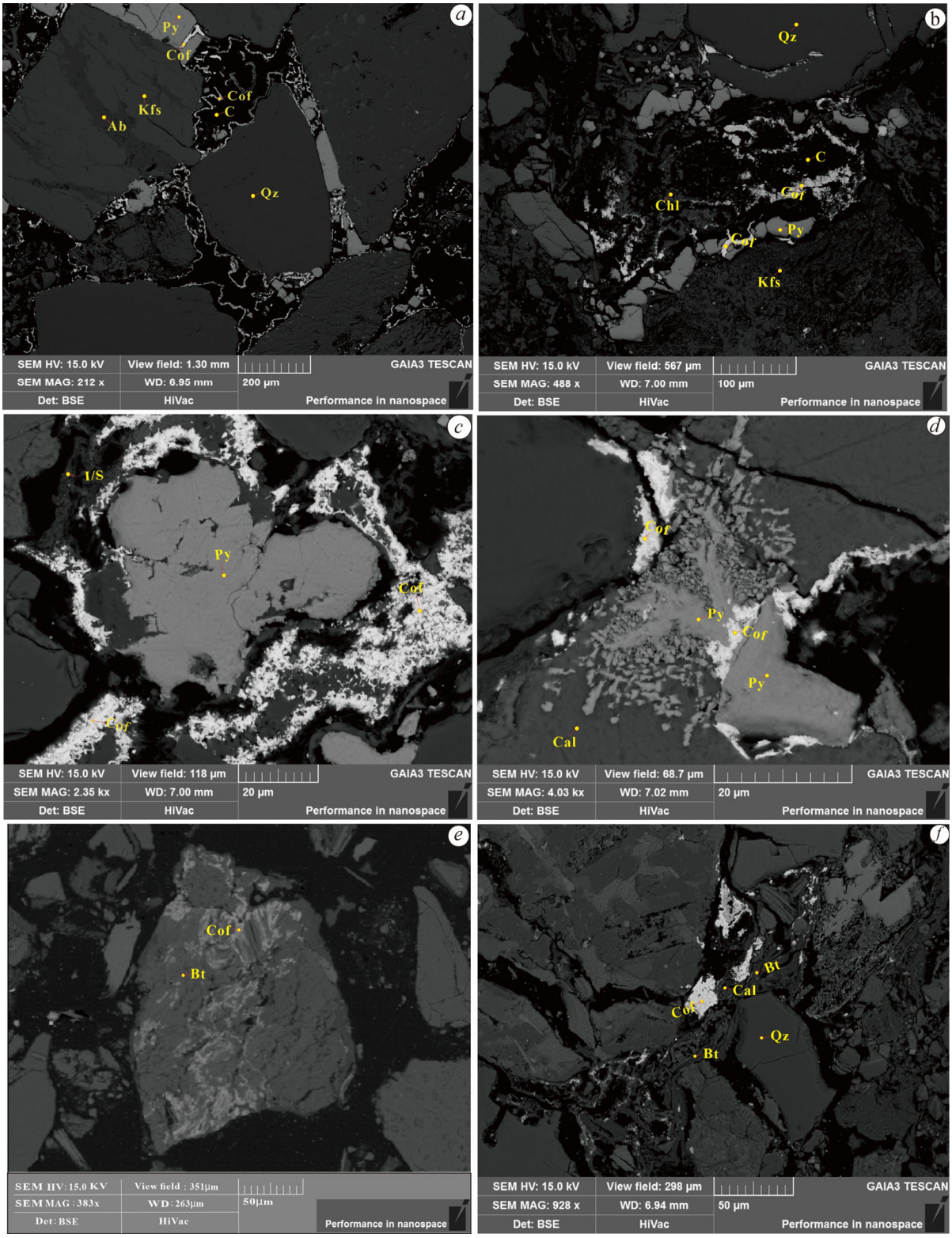


Figure 5. Characteristics of associated minerals with uranium minerals in ore-bearing sandstone of the Zhiluo Formation in the Saitai area. (**a**) Relationship between charcoal and uranium minerals; (**b**) Relationship between chlorite surrounding charcoal and uranium minerals; (**c**) Relationship among authigenic pyrite, illite–smectite mixed layer and uranium minerals; (**d**) Relationship between colloform pyrite in dissolved calcite and uranium minerals; (**e**) Relationship between biotite and uranium minerals; (**f**) Relationship among calcite, biotite and uranium minerals. Qz—Quartz; Ab—Albite, Chl—Chlorite; Bt—Biotite; Cal—Calcite; Py—Pyrite; C—Carbonaceous; Cof—Coffinite.

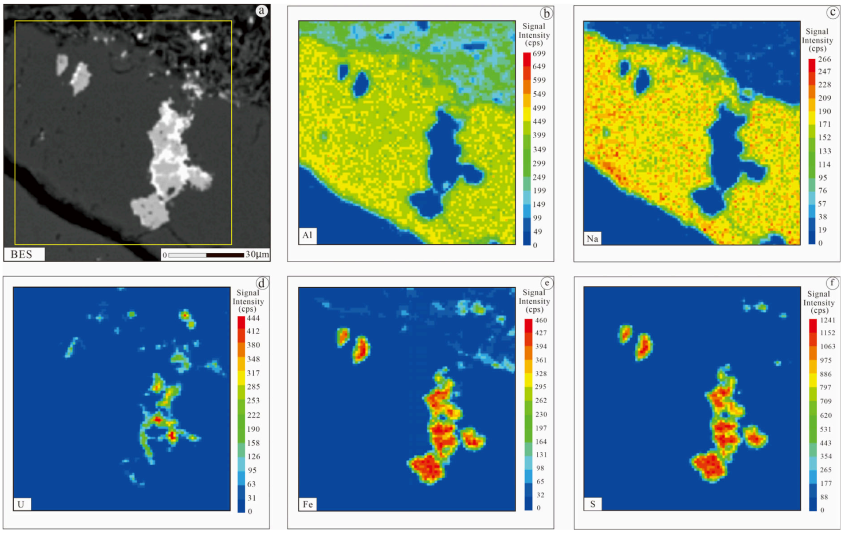


Figure 6. BSE image and EPMA elemental distribution maps of the uranium-mineralized assemblage. (**a**) BSE image, where the yellow rectangle marks the region selected for elemental mapping; (**b**) Al signal intensity map; (**c**) Na signal intensity map; (**d**) U signal intensity map; (**e**) Fe signal intensity map; (**f**) S signal intensity map. Scale bar = 30 μm for all panels.

4.2. Geochemical Characteristics

Gray sandstone samples from the Zhiluo Formation have SiO_2 contents ranging from 60.32 to 75.85% with an average of 70.81%; Al_2O_3 content ranges from 9.94 to 16.82% wt.% with an average of 12.77%; CaO shows the most data dispersion, ranging from 0.42% to 11.23%; and LOI also exhibits considerable variability. K_2O is consistent at 2.75%~3.26%, but Na_2O varies more, ranging from 1.60 to 3.87% (wt.%) (Table 2). Both FeO and Fe_2O_3 are detected in the samples. Fe_2O_3 shows a broad compositional range, and MnO is associated with iron-bearing components. MgO and P_2O_5 both show only slight overall fluctuations. Collectively, these data indicate prominent compositional heterogeneity among samples.

Table 2. Major-element contents of ore-bearing sandstones in the Zhiluo Formation.

Samples	SiO_2 /10^{-2}	Al_2O_3 /10^{-2}	Fe_2O_3 /10^{-2}	FeO /10^{-2}	CaO /10^{-2}	MgO /10^{-2}	K_2O /10^{-2}	Na_2O /10^{-2}	TiO_2 /10^{-2}	P_2O_5 /10^{-2}	MnO /10^{-2}	LOI /10^{-2}
U1/S	72	12.39	2.7	1.30	0.72	1.44	2.91	1.94	0.68	0.088	0.056	3.62
U2/S	60.32	9.94	0.95	0.78	11.23	1.04	2.75	1.6	0.22	0.039	0.083	10.96
U3/S	73.18	12.21	1.26	1.02	1.36	1.32	3.2	2.04	0.33	0.063	0.039	3.84
U4/S	72.83	13.19	0.81	1.26	0.69	1.16	3.22	2.97	0.51	0.058	0.025	3.13
U5/S	73.80	12.22	0.94	1.52	0.87	1.37	3.19	2.44	0.37	0.054	0.032	3.00
U6/S	73.75	12.48	1.05	1.10	0.76	1.28	3.16	2.59	0.41	0.065	0.027	3.19
U7/S	71.2	13.47	1.06	1.85	0.68	1.69	3.24	2.31	0.63	0.088	0.034	3.51
U8/S	73.32	12.77	0.92	1.32	0.73	1.35	3.26	2.53	0.49	0.073	0.03	3.06
U9/S	72.19	12.73	0.74	1.22	0.97	1.02	3.09	3.29	0.48	0.076	0.037	3.99
U10/S	68.88	11.90	3.08	1.26	1.88	1.08	2.90	2.90	0.40	0.076	0.042	5.40
U11/S	73.45	13	0.89	1.25	0.47	1.2	3.21	3.11	0.33	0.07	0.022	2.85
U12/S	75.41	12.14	0.57	1.25	0.56	1	3.1	3.17	0.36	0.078	0.022	2.19
U13/S	75.85	12.15	0.009	1.58	0.42	0.96	3.18	3.17	0.29	0.07	0.016	2.13
U14/S	73.21	13.03	0.66	1.02	0.79	0.97	3.21	3.49	0.52	0.088	0.027	2.86
U15/S	66.78	12.15	0.52	1.39	5.04	1.32	2.98	2.86	0.40	0.060	0.17	6.16
U16/S	64.95	16.22	1.61	3.11	0.53	2.65	2.88	2.22	0.79	0.1	0.033	4.54
U17/S	73.97	12.87	0.56	1.04	0.6	0.82	3.15	3.87	0.38	0.06	0.02	2.54
U18/S	64.11	11.9	5.36	1.15	3.31	1.02	2.87	2.75	0.38	0.089	0.1	6.60
U19/S	71.91	12.44	0.82	1.25	1.75	1.47	3.19	2.01	0.51	0.073	0.076	4.30
U20/S	74.68	12.10	0.56	1.22	0.81	1.30	3.20	2.06	0.33	0.060	0.031	3.48
U21/S	61.23	16.82	3.29	3.18	0.63	2.86	2.95	1.81	0.83	0.18	0.038	5.80

Total organic carbon contents within ore-bearing intervals of the Zhiluo Formation vary from 0.026% to 3.35%, sulfide sulfur contents range from 3.4 × 10^{-6} to 83.3 × 10^{-6}, and Fe^{2+}/Fe^{3+} ratios vary from 0.70 to 92.35, equivalent to Fe^{2+}/total Fe (Fe_T) of 0.41–0.99 (Figure 7).

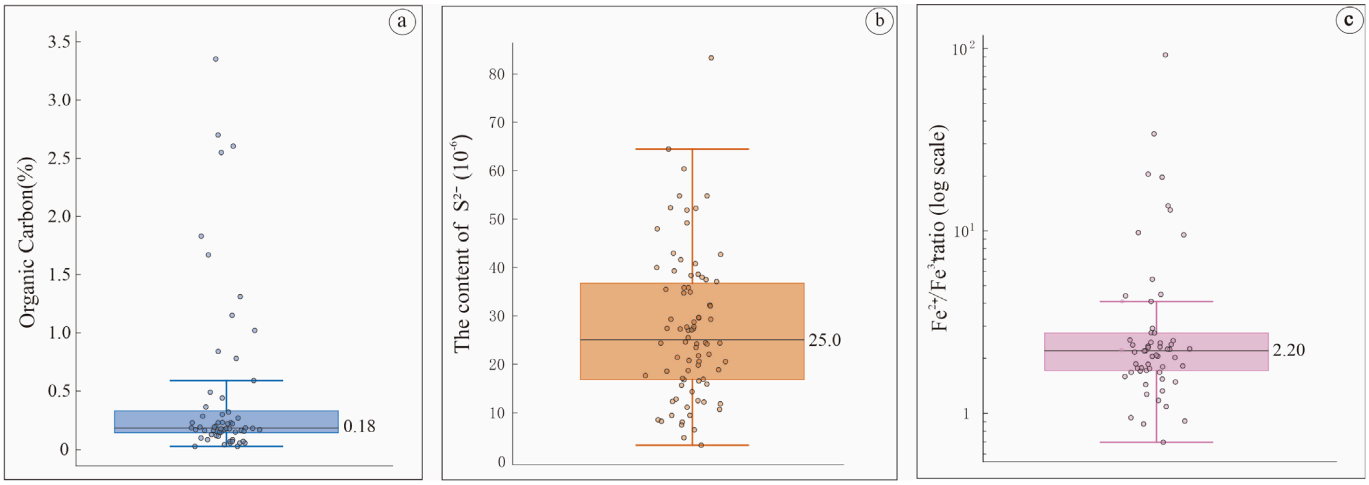


Figure 7. Boxplots showing the distributions of (**a**) Organic Carbon (TOC), (**b**) S^{2-}, and (**c**) Fe^{2+}/Fe^{3+} ratios in the studied samples. In each box plot, the horizontal line denotes the median, the box boundaries indicate the first and third quartiles, and the dashed lines extend to the most extreme data points within 1.5 times the interquartile range (IQR) from the quartiles. For Fe^{2+}/Fe^{3+}, the y-axis is presented on a logarithmic scale to better resolve variations.

The total sulfur content is mostly between 0.1% and 0.3%, and a few samples reach as high as 1.70% (Figure 8). In addition, the data show a positive correlation, suggesting a possible link between sulfur cycling and uranium enrichment rather than a direct causal relationship.

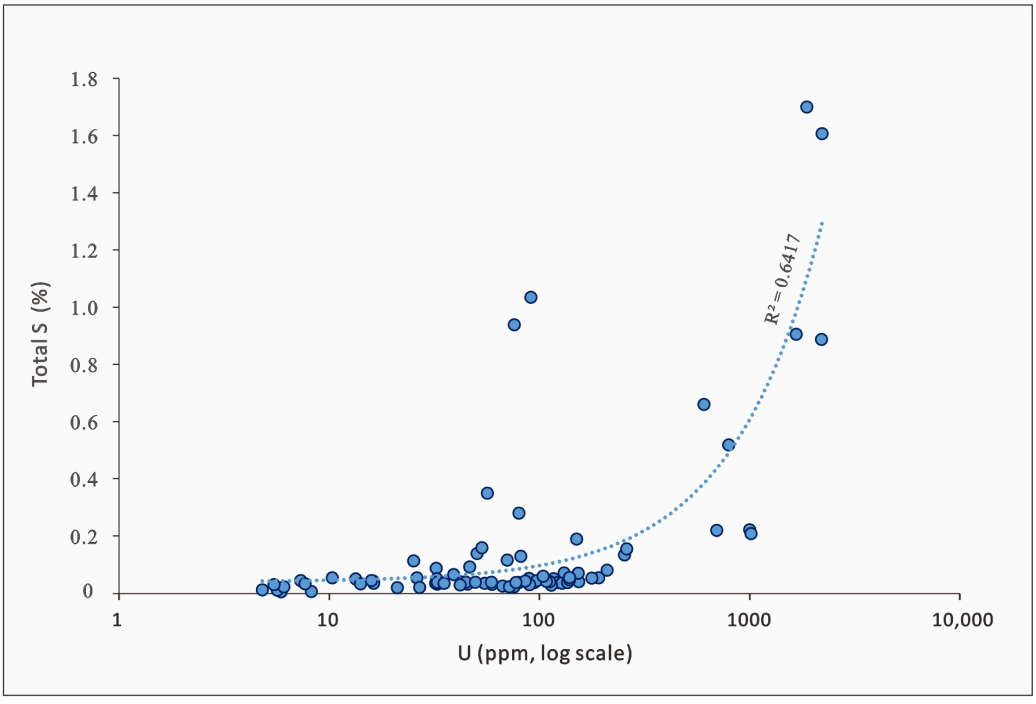


Figure 8. Correlation between uranium concentration and total sulfur content.

In this work, NASC (North American Shale Composite) (La = 32 × 10^{-6}, Ce = 73 × 10^{-6}, Pr = 7.9 × 10^{-6}) [36] was used for REE normalization to remove the interference of terrigenous clastic input with Ce anomaly signals. Ce/Ce* ratios for ore-bearing sandstones of the Zhiluo Formation range from 0.72 to 1.01 (Table 3). According to the discrimination thresholds (positive anomaly > 1.1, negative anomaly < 0.9), most samples exhibit negative Ce anomalies, with values as low as 0.72, which means that the depositional environment was predominantly reducing, with a transitional trend toward suboxic conditions.

Table 3. Key rare earth element parameters and Ce/Ce* values (NASC-normalized) of ore-bearing sandstone samples from the Zhiluo Formation.

Samples	La	Ce	Pr	Ce/Ce*
U1/S	84.4	83	8.61	0.724
U2/S	19.2	31.8	4.18	0.834
U3/S	24.7	48.6	5.83	0.952
U4/S	35.5	53.6	5.3	0.918
U5/S	21.2	39.5	4.44	0.957
U6/S	26.3	45.2	4.93	0.933
U7/S	30.3	53.5	5.68	0.958
U8/S	28.3	46.8	4.66	0.958
U9/S	19.1	43.9	5.51	1.006
U10/S	35.9	63.1	5.96	1.014
U11/S	25.7	43.3	4.95	0.902
U12/S	27.7	51	5.89	0.938
U13/S	23.8	42.6	4.86	0.931
U14/S	36.9	70.2	8.31	0.942
U15/S	30.6	60.2	7.22	0.952
U16/S	55.4	104	12.2	0.940
U17/S	22.8	45.4	5.47	0.955
U18/S	33.5	127	31.5	0.919
U19/S	30.3	55.3	6.26	0.944
U20/S	25.2	48.2	5.42	0.969
U21/S	56.5	104	13.1	0.898

To further constrain redox conditions for uranium mineralization, this study also performed uranium valence state analysis on the ore-bearing samples of the Zhiluo Formation from the Saitai area. The U(IV)/U(VI) ratios vary between 0.625 and 34.78, with a mean of 10.89, corresponding to U(IV)/total U ratios of 0.38–0.97 (mean = 0.88) (Figure 9). The high ratio of reduced to oxidized uranium species indicates that uranium mineralization occurred under reducing conditions.

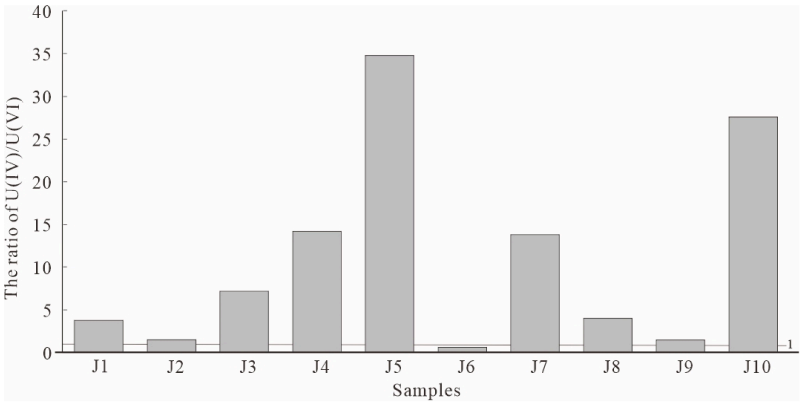


Figure 9. Comparison of uranium valence states in ore-bearing sandstones of the Zhiluo Formation in the Saitai area. The horizontal black line at y = 1 is the reference baseline of the U(IV)/U(VI) ratio.

Secondary fluid inclusions in ore-bearing sandstones of the Zhiluo Formation are hosted in fracture-crosscutting quartz, feldspar microfractures, intergranular calcite, and zeolite (Figure 10). Two distinct fluid inclusion assemblages (FIAs) are identified in quartz. These vapor–liquid inclusions range from 2 × 3 to 7 × 18 μm, with vapor–liquid ratios predominantly ranging from 5% to 10%. Inclusions hosted by intergranular calcite exhibit smaller dimensions and lower vapor proportions.

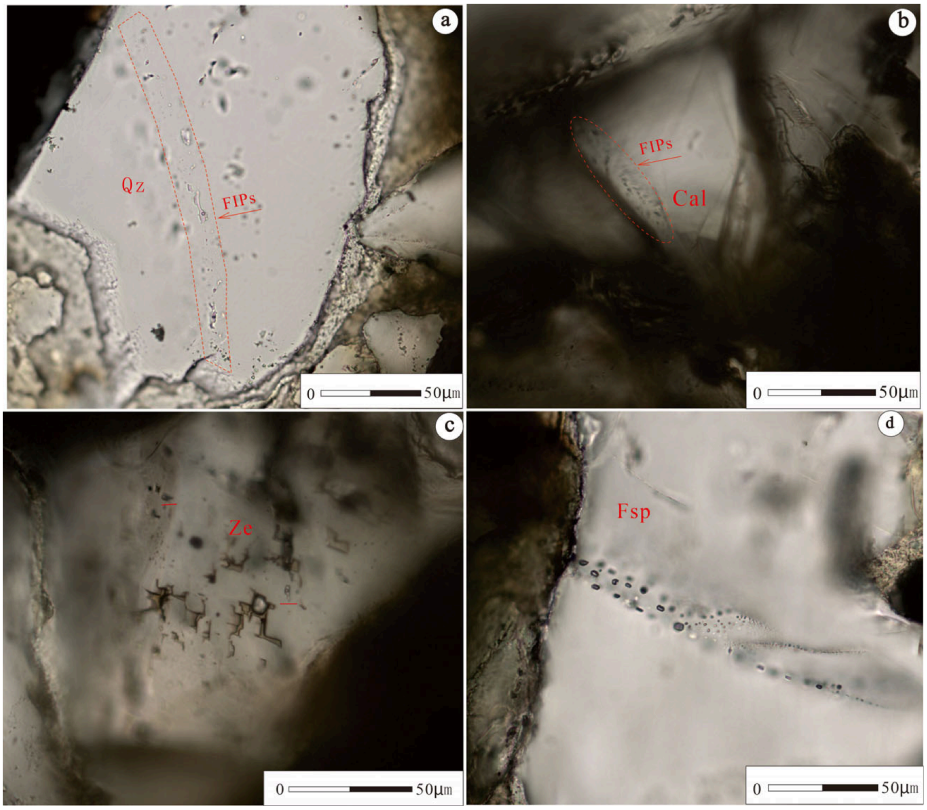


Figure 10. Photomicrographs showing petrographic features of fluid inclusion assemblages (FIAs) in ore-bearing sandstone of the Zhiluo Formation. (**a**) Saline aqueous FIAs along healed microfractures within quartz (Qz); (**b**) Banded FIAs hosted in intergranular calcite (Cal); (**c**) Saline aqueous FIAs within zeolite (Ze); The marked red lines indicate vapor-liquid two-phase fluid inclusions (**d**) Monophase gas inclusions in microfractures of feldspar (Fsp).

Fluid inclusions are classified into four types according to their petrographic features (Table 4). The ore-forming fluids ultimately homogenized to the liquid phase. For all fluid inclusions with paired Th and Tm ice data, homogenization temperatures vary from 130 to 220 °C, ice-melting temperatures vary from −6.2 to −0.5 °C, and salinities range from 0.9 to 9.5 wt.% NaCl equivalent. Based on petrographic characteristics, the measured data were grouped. Zeolite-hosted inclusions and the low-salinity subgroup in quartz microfracture planes were excluded from the syn-mineralization fluid statistics. The syn-mineralization fluid yields homogenization temperatures of 130–183 °C, ice-melting temperatures of −6.2 to −1.6 °C, and salinities of 2.7–9.5 wt.% NaCl equivalent [37]. Microthermometric results differ among host minerals. In intergranular calcite, homogenization temperatures are tightly clustered at 130–138 °C. Four discrete data clusters are recognized on the Tm, ice–Th crossplot (Figure 11). Inclusions from quartz microfracture planes form low- and high-salinity groups. Laser Raman spectroscopic analyses reveal that the vapor phase of these inclusions consists mainly of CO_2 (Figure 12).

Table 4. Homogenization temperature and salinity of fluid inclusions from ore-bearing sandstones of the Zhiluo Formation, Saitai area.

Host Mineral/Occurrence	Size (μm)	Vapor/Liquid Ratio (%)	Th (°C)	Tm,ice (°C)	Salinity (wt% NaCl Equiv)
Microfractures cutting quartz grains	3 × 15	5~10	161	−1.6	2.7
	20 × 40	5~10	172	−2.6	4.3
	6 × 10	5~10	180	−2.7	4.5
	4 × 7	5~10	183	−2.7	4.5
	4 × 18	5~10	164	−2.5	4.2
	5 × 12	5~10	181	−2.5	4.2
	4 × 8	≤5	87	–	–
	4 × 20	≤5	101	–	–
	3 × 6	≤5	135	–	–
	7 × 18	≤5	101	–	–
	4 × 6	≤5	103	–	–
Microfracture planes in quartz grain	2 × 4	5–10	180	−6.1	9.3
	3 × 3	5–10	160	−6.1	9.3
	3 × 4	5–10	171	−6.2	9.5
	5 × 8	5–10	160	−0.5	0.9
	2 × 3	5–10	155	−0.5	0.9
	2 × 4	5–10	162	−0.6	1.1
Calcite filling intergranular pores	2 × 3	≤5	135	−3.6	5.9
	2 × 2	≤5	138	−3.6	5.9
	2 × 3	≤5	133	−3.7	6.0
	2 × 3	≤5	133	−3.7	6.0
	2 × 3	≤5	130	−3.6	5.9
Zeolite filling intergranular pores	2 × 5	10~15	220	−5.4	8.5
	3 × 5	≤5	146	−5.5	8.6
	3 × 8	5~10	178	–	–

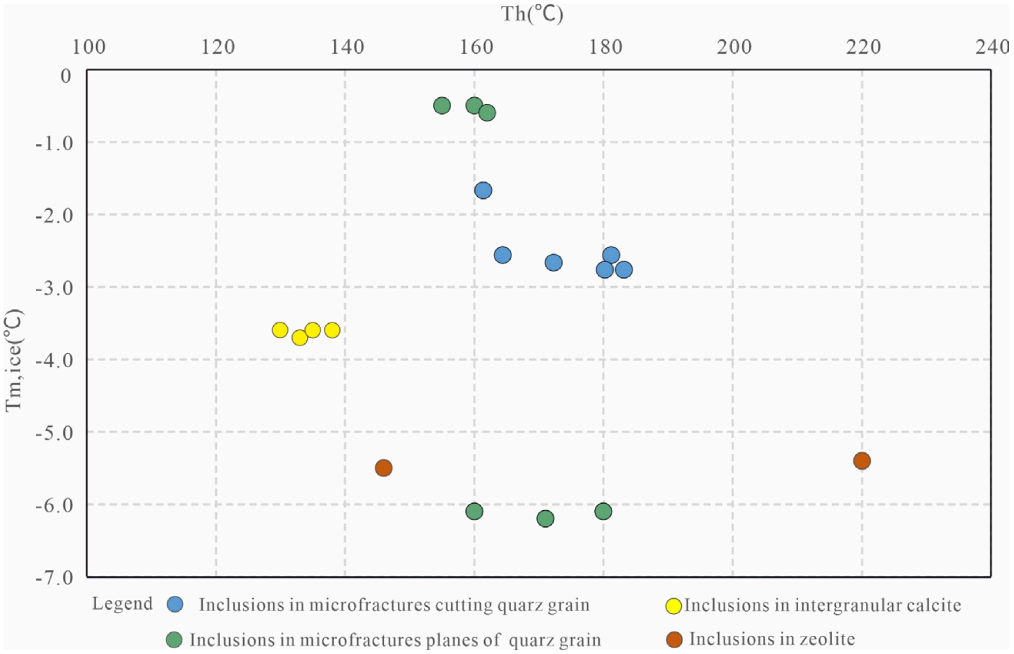


Figure 11. Tm,ice versus Th scatter plot of fluid inclusions from the Zhiluo Formation ore-bearing sandstones.

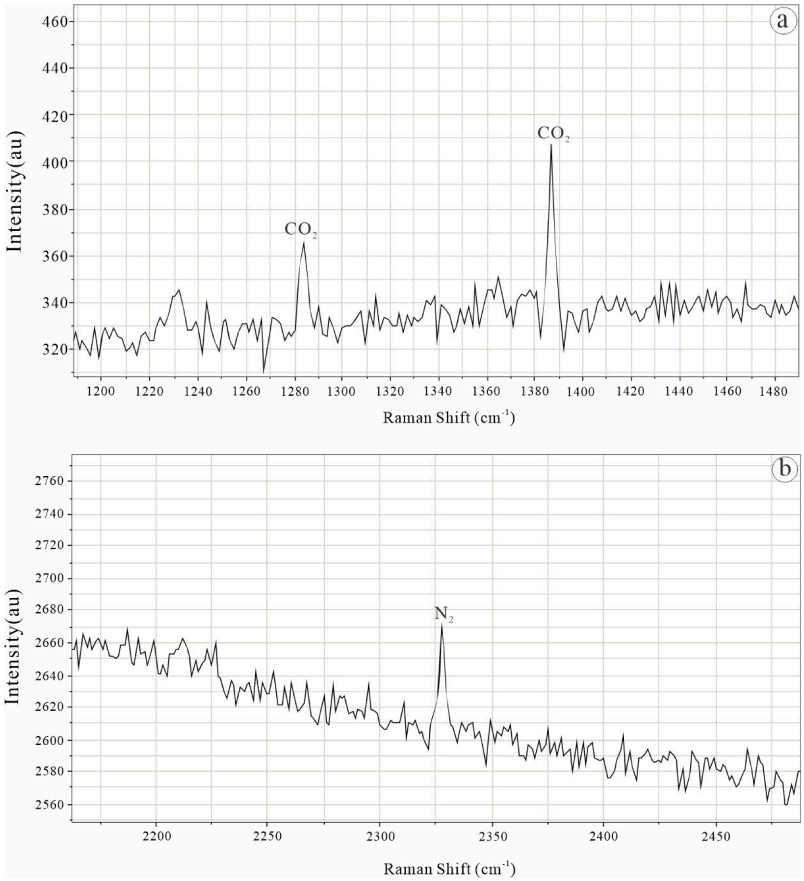


Figure 12. Laser-Raman spectra of vapor phases from fluid-inclusion in ore-bearing sandstones of the Zhiluo Formation. (**a**) Raman spectrum showing CO_2 peaks; (**b**) Raman spectrum showing N_2 peak.

5. Discussion

5.1. Fluid Evolution Recorded by Mineral Assemblages

Redox and pH conditions are decoupled in this uranium mineralization system; pH remains alkaline while redox states vary among different fluid episodes [10,38]. The ore-bearing horizon in the Saitai area corresponds to the Middle Jurassic Zhiluo Formation. This target ore-hosting layer has a steady lateral growth and is rich in reducing media such as carbonaceous debris, pyrite, and biotite. Among them, carbonaceous debris is the primary reducing material, whereas authigenic pyrite exerts only limited control on uranium enrichment. The coexistence of carbonaceous debris and syn-sedimentary authigenic pyrite records the primary sedimentary reducing background.

Combined with FIA petrography and mineral paragenetic relationships, three fluid episodes are recognized in the Zhiluo Formation ore-bearing sandstone. The first episode is recorded by liquid-rich aqueous FIAs along healed quartz microfractures with well-developed FIPs. Microthermometric data indicate a medium-temperature saline fluid event accompanied by inferred weakly alkaline fluid–rock interaction. This phase of fluid activity drove widespread feldspar and carbonate dissolution within the sandstone reservoir. The second episode is documented by FIAs in intergranular calcite. Crosscutting textures show that calcite formed later, representing a subsequent cooler fluid event after the main hydrothermal activity. The third episode is represented by aqueous and hydrocarbon FIAs in late diagenetic zeolite. This event occurred after calcite cementation, marking the final stage of basin fluid evolution. In summary, the fluid system evolved sequentially from medium-temperature fluids with inferred weakly alkaline fluid–rock interaction, through cooler post-hydrothermal activity, to late low-temperature diagenetic alteration.

The relationship between this fluid evolution sequence and uranium mineralization is discussed in the following section.

Geochemical analyses show that the sandstones of the lower part of the Zhiluo Formation have relatively high total organic carbon and total sulfur contents, with a strong positive correlation between sulfur and uranium. The sandstones are also characterized by high S^{2-} concentrations, elevated Fe^{2+}/Fe^{3+} ratios, an overall absence of positive Ce anomalies (Ce anomalies are normal to slightly negative), and generally high U(IV)/U(VI) ratios. All this evidence indicates that the fluids associated with ore-bearing gray sandstones existed under strongly reducing conditions.

Abundant uranium minerals are adsorbed onto the margins of carbonaceous debris, and some chlorite and secondary carbonate minerals coexist with uranium minerals (Figure 5d), indicating predominantly alkaline fluid activity. Petrographic BSE observations show that coffinite is spatially associated with patchy chlorite derived from partial alteration of detrital K-feldspar. Coffinite fills adjacent intergranular pores without replacing or cutting chlorite, indicating that chlorite formed in early diagenesis before uranium mineralization. Local chloritization modulates pore surface properties and Eh-pH conditions to form favorable microenvironments for coffinite precipitation. This confirms that chlorite is not an authigenic phase coeval with uranium mineralization. Carbonate minerals, colloform pyrite, and coffinite jointly occupy dissolution sites in feldspar and carbonate grains. Clustered epigenetic pyrite is also found in intragranular dissolution pores of K-feldspar and albite. Colloform pyrite similarly occurs in micropores formed by biotite alteration and carbonate dissolution (Figure 13).

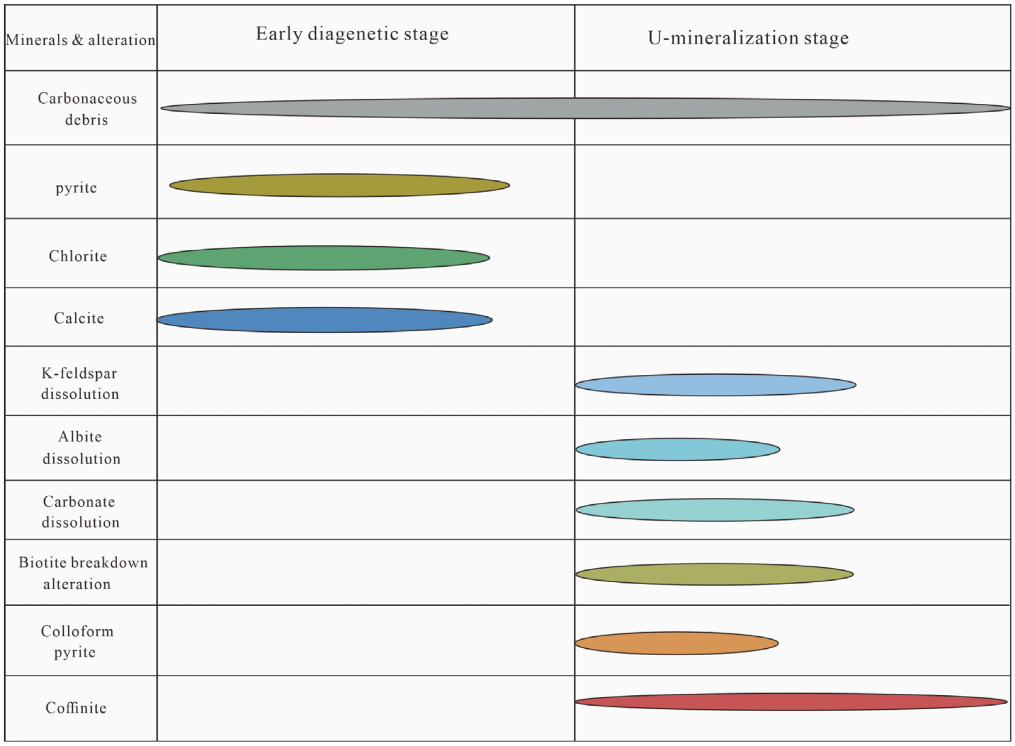


Figure 13. Paragenetic sequence of minerals and alteration events related to uranium mineralization. For carbonaceous debris, the horizontal bar represents its persistence interval rather than formation timing.

In the northern Ordos Basin, infiltrating water in Zhiluo Formation sandstones is alkaline, with maximum paleotemperatures below 70 °C [29]. Fluid inclusion analyses were performed on carbonate minerals, quartz fractures, and zeolites. These results reveal medium–low temperature CO_2-bearing saline inclusions. This suggests that the

ore-bearing sandstones were overprinted by medium-temperature fluids. The fluids existed under inferred weakly alkaline conditions. These basinal fluids sourced from the Permian sedimentary strata in this region are generally alkaline and characterized by elevated salinity [39], and the Bojianghaizi and Sanyanjing faults south of the study area may connect the Zhiluo Formation with deeper strata [40]. The occurrence of coffinite itself indicates reducing conditions, but does not by itself demonstrate that the ore-forming fluid was capable of reducing dissolved U(VI) to U(IV). In this system, pyrite and sedimentary organic matter are the primary electron donors [13]. Under the inferred shallow-burial, low-temperature [41], near-neutral to weakly alkaline conditions, pyrite can act as a reductant for U(VI). Although pyrite is thermodynamically stable under weakly alkaline bulk conditions, oxidation at grain surfaces by incoming oxidizing fluids (containing dissolved O_2 and U(VI)) releases electrons and generates localized microdomains. These microscale environments lower the local pH, enhancing the rate of pyrite oxidation and providing the kinetic conditions required for U(VI) reduction [42]. The coupled reaction of pyrite oxidation and U(VI) reduction can proceed within this window and kinetically feasible at low temperatures. In addition, disseminated organic matter in host sandstones serves as an additional electron donor, further facilitating U(VI) reduction. The combination of pyrite and organic matter provides sufficient reducing capacity to drive U(VI) reduction and coffinite precipitation [13].

Previous work on alkaline fluid dissolution [43,44] shows that, under the influence of deep-derived, medium-temperature fluids in the Saitai area, hydroxyl (OH^-) activity in alkaline fluids accelerates markedly: Al in the feldspar crystal framework is complexed by hydroxyl groups to form Al $(OH)_4{}^-$, while Na^+ and K^+ are released into the fluid. This mechanism readily accounts for the observed mineral assemblages and geochemical signatures. Overall, shallow oxidized alkaline fluids and deep-derived alkaline reducing fluids both entered the reservoir sandstones and reacted with carbonaceous debris and pyrite, establishing an overall reducing–alkaline environment locally characterized by feldspar dissolution, biotite alteration, carbonate dissolution, colloform pyrite, chloritization, and zeolite.

5.2. Roles of Different Reducing Media in Uranium Mineralization

Different geological bodies in the Wulashan-Langshan area in the northern Ordos Basin tend to have higher uranium abundance [45]. Large-scale Archean–Paleoproterozoic crystalline rock sequences and granitoid intrusions of various ages are found throughout this provenance [46]. The Zhiluo Formation in the Saitai area is mainly a southwest-dipping monoclinal structure with some local minor uplifts. The persistent stratigraphic dip exerted a key control on subsequent fluid migration within the uranium-bearing reservoir. Geochemical data show that total sulfur content is positively correlated with uranium, and secondary pyrite is closely associated with uranium mineralization. Microbially mediated U(VI) reduction can take place in organic-rich sedimentary basins accompanied by sulfate reduction [47]. Our petrographic and microscopic observations reveal that uranium minerals are predominantly concentrated at carbonaceous debris, highlighting the dominant role of in situ organic reductants; such microbial processes may locally occur at sites with well-developed secondary pyrite. Oxygen- and uranium-bearing meteoric waters have moved into the Zhiluo Formation in the northern Ordos Basin through seepage and runoff in the Yimeng uplift. After entering the Zhiluo Formation in Saitai, these fluids met reducing media consisting of carbonaceous debris, pyrite, and biotite, thus causing uranium enrichment. Deep-derived medium-temperature fluids also carry reduced species [20,29]. Macroscopically, the geometry of orebodies is constrained by gray sandstones rich in coal detritus and pyrite. Lateral variations in orebodies are relatively stable and broadly

concordant with stratigraphic bedding. Microscopically, uranium minerals occur mainly around organic matter and authigenic pyrite, and within alkaline medium–low temperature dissolution pores or fractures in biotite, feldspar, or carbonate cements. Combined with the mineral fluid response signatures, this study proposes a genetic uranium mineralization model controlled by reducing media for the Saitai area (Figure 14).

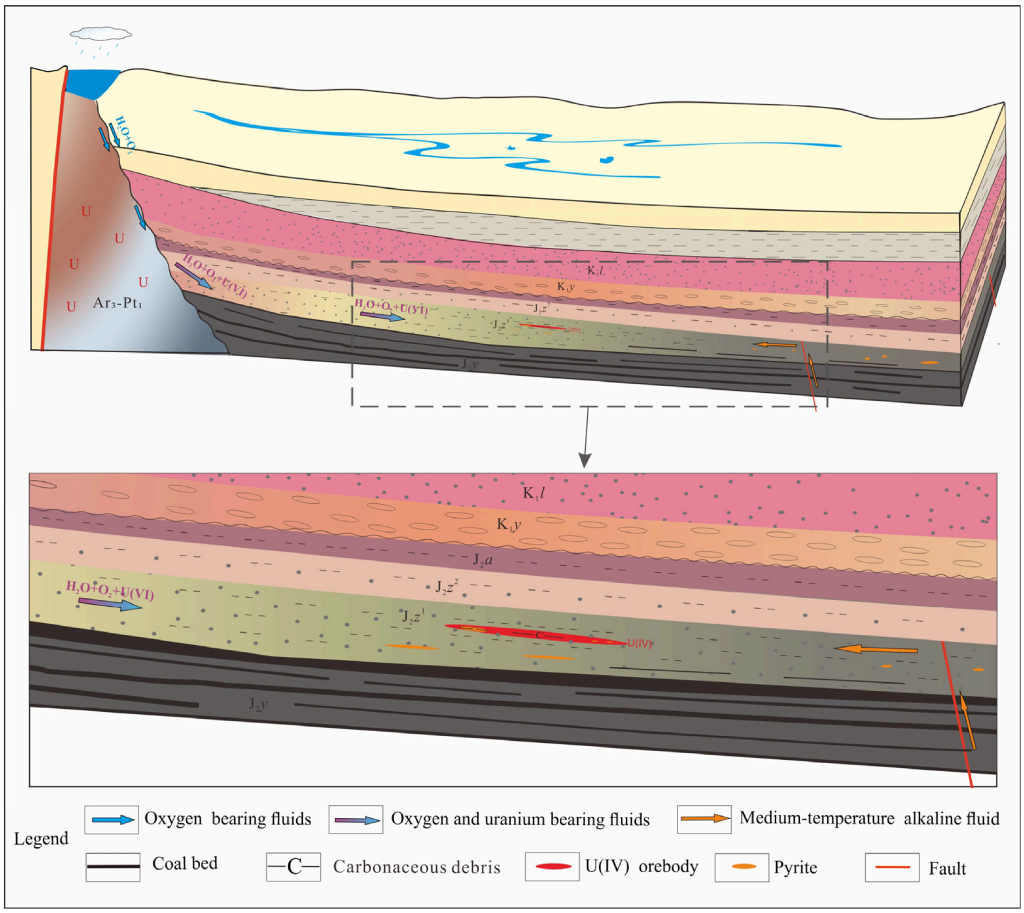


Figure 14. Uranium metallogenic model map of the Saitai area, Ordos Basin. J_2y—Yan'an Formation, J_2z^1—Lower member of Zhiluo Formation, J_2z^2—Upper member of Zhiluo Formation, J_2a—Anding Formation), K_1y—Yijun Formation, K_1l—Luohe Formation.

The paragenetic relationship between authigenic pyrite and uranium minerals is highly variable in the study area. Uranium mineralization is commonly associated only with pyrite and carbonaceous debris. In contrast, authigenic pyrite, which forms in pure pore spaces and lacks carbonaceous debris, is less likely to host uranium minerals. This indicates that pyrite–uranium coupling is largely controlled by organic matter derived from carbonaceous debris. As a type of reactive solid organic substance, carbonaceous debris can also adsorb and reduce uranium at the same time [48,49]. Microscopic observations reveal that uranium minerals attach to the surface of carbonaceous material and fill pores. When U^{6+}-bearing oxidizing groundwater flows through carbonaceous-rich sandstones, carbonaceous debris supplies electrons that reduce soluble U^{6+} to insoluble U^{4+} and trigger uranium mineral precipitation.

Medium- to low-temperature alkaline fluids in the study area induce partial dissolution of silicate and carbonate minerals, developing abundant intragranular and intergranular dissolution pores and fracture systems that provide favorable reservoir and reaction spaces for uranium mineralization. Petrographic observations reveal that colloidal pyrite is closely associated paragenetically with uranium minerals, which are predominantly

concentrated within feldspar dissolution cavities. Microscopic spatial coupling of Fe, S, and U elements effectively records the grain-scale microenvironment of uranium mineralization. The strong positive U–total S correlation, together with elevated S^{2-} concentrations, could be consistent with sulfate reduction within local pore systems. This process generates hydrogen sulfide, which releases hydrogen ions during subsequent redox reactions and enhances the capacity of pyrite to reduce hexavalent uranium [50,51]. Altered biotite retains abundant structural Fe^{2+} in its crystal lattice. When oxidizing uranium-bearing fluids infiltrate the altered and decomposed rock system, structural Fe^{2+} in biotite is oxidized to Fe^{3+}. Meanwhile, aqueous U(VI) in the fluids is synchronously reduced to U(IV), which eventually precipitates and accumulates within dissolution pores to complete the uranium mineralization process.

5.3. Divergent Metallogenesis of Typical Uranium Ore Fields in Northern China

In contrast, the petrographic and mineralogical observations suggest that uranium mineralization formed within reducing sand bodies. Carbonaceous debris, together with fine-grained pyrite, serves as the primary in situ reductant to trigger U(VI) reduction and uranium mineral precipitation. Hydrocarbon-bearing fluids may have induced late diagenetic alteration but are not considered the principal reductant for the main uranium mineralization in our study area. This interpretation does not invalidate the hydrocarbon-related fluid model for other parts of the Ordos Basin but indicates that redox reactions controlled by intrinsic reducing materials in sandstone were dominant at our study site.

Uranium deposits are closely associated with reducing media such as organic matter, pyrite, and biotite in Mesozoic–Cenozoic coal-bearing basins in northern China. Due to different sedimentary conditions and tectonic activities, different reducing media and metallogenic characteristics develop in different ore fields. This study compares typical uranium deposits from two major basins: Saitai and Tarangaole from the Ordos Basin, and Baiyanhua from the Erlian Basin [5,30,49,52–54], to constrain how reducing media influence sandstone-hosted uranium mineralization.

These deposits have similar ore-forming fluid features. The main uranium mineralization is due to meteoric water-derived oxygen- and uranium-rich fluids, which carry uranium as uranyl carbonate complexes that precipitate via redox reactions. All three deposits belong to an in situ reduction metallogenic system hosted within coal-bearing sequences. Coal-bearing strata supply primary reducing materials, whereas reducing media within sand bodies are derived from in situ organic detritus; no pre-ore reservoir modification by exogenous fluids is needed. Orebodies are stratabound in permeable sandstones and controlled by sandstone–mudstone interbedded assemblages.

Despite this shared metallogenic framework, the three ore fields display pronounced differences in sedimentary conditions, tectonic activities, and thus in reducing media and metallogenic characteristics. Both the Saitai and Tarangaole deposits occur in Middle Jurassic Zhiluo Formation fluvial sand bodies under a regional tectonic uplift setting, yet their divergent sedimentary microfacies resulted in different reductant assemblages: uranium enrichment at Saitai is dominated by carbonaceous debris and superimposed by medium–low temperature alkaline fluids, whereas Tarangaole mineralization is closely coupled with organic matter, framboidal and colloform pyrite, and ilmenite under low-temperature hydrocarbon-rich reducing fluids. In contrast, the Baiyanhua deposit developed under Cenozoic tectonic subsidence and faulting, with a complex fluvial–delta–shallow lacustrine succession in the Saihan Formation; it records early uranium pre-enrichment by coal and lithic fragments followed by later overprinting by hydrocarbon fluids.

In short, differences in tectono-sedimentary settings control the diversity of reductant assemblages and resultant uranium mineralization across the three deposits.

5.4. Comparison with Existing Genetic Models

Multiple genetic models have been proposed for uranium mineralization in the Zhiluo Formation of the Ordos Basin [55]. Among them, Xue and Chi [16] proposed fluid mixing between descending U-bearing meteoric water and ascending hydrocarbon-rich brines, in which hydrocarbons acted as reductants; ore precipitation was controlled by mixing at fluid interfaces rather than by classic roll-front processes. Cai et al. [47] suggested a microbial mechanism: sulfate-reducing bacteria oxidize petroleum to produce H_2S that reduces U(VI). Jiao et al. [27] put forward a dual reducing medium model, emphasizing syn-sedimentary carbonaceous fragments as primary in situ reductants that work together with extrinsic hydrocarbon fluids. Besides organic and hydrocarbon reductants, Ding et al. [56] identified a non-microbial pathway: altered ilmenite-derived TiO_2 minerals concentrate uranium via adsorption and radiation-driven catalytic reduction.

This study establishes a reasonable metallogenic interpretation for uranium mineralization in the Saitai area. Microscopic BSE observations and whole-rock geochemical results indicate that coffinite is spatially associated paragenetically with carbonaceous debris, and uranium enrichment is more closely linked to organic carbon than to sulfide sulfur. No obvious biogenic structures were identified in uranium-bearing minerals, and pyrite without associated carbonaceous matter is essentially uranium-barren. This phenomenon is consistent with previous experimental findings: abiotic sulfide-driven U(VI) reduction proceeds inefficiently under low-temperature conditions [42,57], whereas solid organic matter can effectively provide adsorption sites for uranium enrichment and electrons for uranium reduction [58].

Distinct from the hydrocarbon-dominated and microbe-mediated metallogenic models summarized for the Dongsheng uranium deposit, uranium mineralization in the Saitai area is predominantly controlled by in situ carbonaceous debris. Locally developed moderate-temperature alkaline fluids mainly improved reservoir pore space, while their potential reducing capacity remains unclear and needs further systematic study. Minor colloform pyrite locally implies limited microbial and sulfide participation, which also requires more geochemical evidence for confirmation.

The metallogenic framework proposed in this study is therefore different from previously established models. Uranium precipitation in the Saitai section was primarily induced by reactions between U-bearing meteoric water and detrital carbonaceous debris, with pyrite serving only as a secondary reductant. This genetic mechanism is regionally limited to the studied Saitai profile and cannot be universally applied to all uranium deposits along the northern Ordos Basin margin.

5.5. Reducing Media-Constrained Metallogenic Model: Application and Prospect

Nevertheless, this study identifies medium–low temperature alkaline fluid activity in the Saitai area through micro-mineralogical observations and fluid inclusion studies. Such fluids enhanced the reducing capacity of the ore-forming system and contributed directly to uranium precipitation. In addition, medium–low temperature alkaline dissolution of feldspar and carbonate minerals created pore space that accommodated subsequent uranium and sulfate enrichment.

Integration of geological and geochemical data indicates that “mud-sand-mud” sandwich structure, carbonaceous-clast-rich intervals, and alkaline-reducing geochemical proxies constitute important indicators for uranium-bearing intervals in the Saitai area. Medium–low temperature alkaline fluid dissolution improved reservoir pore systems and created effective precipitation spaces for later-stage uranium mineralization. This metallogenic model can be used to explain analogous coal-hosted sandstone-type uranium deposits in adjacent and similar basins.

In the Saitai uranium mineralization model, reducing media exert the dominant control. Oxygenated, uranium-bearing fluids primarily transport uranium into the system. Once these fluids encounter reducing media, host rocks are altered under reducing conditions and develop distinct alteration assemblages. It remains unclear how uranium-related alteration patterns control mineralization. This issue needs to be disentangled from both mineral assemblage and geochemical perspectives. Only then can the metallogenic regularities be fully resolved. We also note that microscale water–rock interactions within carbonaceous debris remain poorly constrained and would benefit from additional in situ geochemical analyses.

6. Conclusions

(1) The Zhiluo Formation ore-bearing intervals in the Saitai area, Ordos Basin, display a clear "mud-sand-mud" sandwich structure. Reducing media—carbonaceous debris, pyrite, and biotite clasts—are readily visible in the ore-hosting sandstones. Uranium minerals mostly line the margins of pyrite, carbonaceous debris, and biotite. They adsorb tightly onto organic-rich debris and show partial paragenesis with associated phases. Authigenic pyrite, when associated with organic matter, also occurs alongside uranium minerals. Colloform pyrite further coexists with uranium in feldspar and carbonate dissolution pores.

(2) The paragenetic assemblage of uranium minerals, together with geochemical data on major elements, organic matter, total sulfur content, S^{2-}, Fe^{2+}/Fe^{3+}, Ce anomalies, uranium valence states, and fluid inclusions, points to an alkaline-reducing fluid environment. Deep, medium–low temperature alkaline fluid activity also overprinted the system.

(3) The margins of carbonaceous debris constitute the main sites of uranium enrichment under alkaline conditions. These bands play a dual role—adsorbing and reducing uranium from oxygenated, uranium-bearing fluids. Authigenic pyrite, by contrast, exerts limited control on uranium mineralization. Medium–low temperature dissolution under inferred alkaline conditions provides partial ore-hosting space for later sulfate-related mineralization. Reducing–alkaline fluid indicators and carbonaceous-debris-rich intervals therefore serve as the primary prospecting guides for uranium mineralization in the Zhiluo Formation of the Saitai area.

Author Contributions: Conceptualization, Q.S. and D.T.; methodology, Q.S. and Z.W.; software, Q.S.; formal analysis, Q.S. and Z.W.; investigation, Q.S., Y.H., C.Z. and J.T.; resources, D.T., Z.W. and X.G.; data curation, Q.S., W.G. and H.D.; writing—original draft preparation, Q.S.; writing—review and editing, Q.S. All authors have read and agreed to the published version of the manuscript.

Funding: This study was supported by China National Key R&D Program (2023YFC2906700); CGN Scientific Research Project (CGNPC-URC-T-2025-13); China Geological Survey Project (DD202402047).

Data Availability Statement: Data are contained within the article. Further inquiries can be directed to the corresponding authors.

Acknowledgments: The authors thank Yinhang Cheng and Reng'an Yu for valuable comments and guidance on this manuscript, Hu Guo for EPMA (electron probe microanalysis) experimental assistance, and Xu Chen and Xueming Teng for support with geological field investigations. During the preparation of this manuscript, the authors used Doubao (doubao.com) for language polishing. The authors have reviewed and edited the output and take full responsibility for the content of this publication.

Conflicts of Interest: Deqiang Tian and Zhaojian Wu are employees of CGNPC Uranium Resources Co., Ltd. Xiaoyu Guo and Jiapeng Tian are employees of Inner Mongolia Coal Construction Engineering (Group) Corporation. The paper reflects the views of the scientists and not the companies.

References

1. Liu, Z.Y.; Li, X.D.; Han, X.Z.; Zhang, B.; Wang, M.T.; Hui, X.C.; Zhao, Y.A. Characteristics of uranium mineralization and identification evaluation on metallogenic environment in Nalinggou region. *World Nucl. Geosci.* **2016**, *33*, 146–156.
2. Li, X.D.; Yi, C.; Gao, H.W.; Han, X.Z.; Liu, Z.; Hui, X.C. Discussion on formation mechanism of paleo-interlayer oxidation zone of Zhiluo Formation in northeastern Ordos Basin. *Geoscience* **2016**, *30*, 739–747.
3. Lu, C.; Jiao, Y.Q.; Peng, Y.B.; Wu, L.Q.; Miao, A.S.; Rong, H.; Xie, H.L. Paleo-interlayer oxidation zone identification and spatial localization prediction in Daying area. *Geol. China* **2018**, *45*, 1228–1240.
4. Ren, Y.S. Study on REE-U Element Metallogenic Mechanism in Northern China: A Case Study of Bayan Obo Fe-REE-Nb Deposit, Sandstone-Type Uranium Deposits in Songliao and Ordos Basins. Ph.D. Thesis, University of Science and Technology of China, Hefei, China, 2019.
5. Peng, S.L.; Tian, J.P.; Guo, X.Y.; Jin, Y.P.; Sun, B.; Dou, H.X.; Zhang, F.; Hao, J.; Hu, Y.L.; Chen, L.; et al. Characteristics and metallogenesis of ore-bearing sandstone in the Tarangaole sandstone-type uranium deposit, Ordos Basin. *Geol. China* **2023**, *50*, 264–276.
6. Cheng, Y.H.; Jin, R.S.; Cuney, M.; Petrov, V.A.; Miao, P.S. The strata constraint on large-scale sandstone-type uranium mineralization in Meso-Cenozoic basins, northern China. *Acta Geol. Sin.* **2024**, *98*, 1953–1976.
7. He, F.; Li, Z.Y.; Liu, X.Y.; Zhang, Z.L.; Wang, L.H.; Liu, C.H.; Zhang, Y.; Qiu, L.F.; Han, M.Z. Study on uranium mineralization mechanism of the Telaobao ore field in northwestern Ordos Basin. *Uranium Geol.* **2023**, *39*, 859–874.
8. Han, M.Z.; Li, Z.Y.; Qiu, L.F.; Zhang, Z.L.; Wang, L.H. Petrological-geochemical characteristics of sandstone in Telaobao uranium deposit of Ordos Basin and their implications for uranium mineralization. *Uranium Geol.* **2025**, *41*, 551–569.
9. Cheng, Y.H.; Jin, R.S.; Wang, S.Y.; Teng, X.M. Two metallogenic models of sedimentary-hosted uranium deposit: Jingchuan and Tale types. *Earth Sci.* **2025**, *50*, 46–57.
10. Kyser, K.; Cuney, M. Sandstone-hosted uranium deposits. In *Geology and Geochemistry of Uranium and Thorium Deposits*; Cuney, M., Kyser, K., Eds.; Mineralogical Association of Canada Short Course: Quebec, QC, Canada, 2015; Volume 46, pp. 225–304.
11. Cumberland, S.A.; Douglas, G.; Grice, K.; Moreau, J.W. Uranium mobility in organic matter-rich sediments: A review of geological and geochemical processes. *Earth-Sci. Rev.* **2016**, *159*, 160–185. [CrossRef]
12. Shamim, A.; Yang, X.Y.; Franco, P. Sandstone type uranium deposits in the Ordos Basin, northwest China: A case study and an overview. *J. Asian Earth Sci.* **2017**, *146*, 367–382. [CrossRef]
13. Bonnetti, C.; Cuney, M.; Michels, R.; Truche, L.; Malartre, F.; Liu, X.D.; Yang, J. The multiple roles of sulfate-reducing bacteria and Fe-Ti oxides in the genesis of the Bayinwula roll front-type uranium deposit, Erlian Basin, NE China. *Econ. Geol.* **2015**, *110*, 1059–1081. [CrossRef]
14. Dahlkamp, F.J. *Uranium Deposits of the World: USA, Latin America, South Africa, Australia, Asia*; Springer: Berlin, Germany, 2009; p. 502.
15. Pirajno, F. *The Geology and Tectonic Settings of China's Mineral Deposits*; Springer: Dordrecht, The Netherlands, 2013; p. 654.
16. Xue, C.J.; Chi, G.X.; Xue, W.T. Interaction of two fluid systems in the formation of sandstone-hosted uranium deposits in the Ordos Basin: Geochemical evidence and hydrodynamic modeling. *J. Geochem. Explor.* **2010**, *106*, 218–231. [CrossRef]
17. Adams, S.S.; Smith, R.B. *Geology and Recognition Criteria for Sandstone Uranium Deposits in Mixed Fluvial-Shallow Marine Sedimentary Sequences, South Texas*; Report GJBX-1(81); U.S. Department of Energy: Grand Junction, CO, USA, 1981; p. 145.
18. Walton, A.W.; Galloway, W.E.; Henry, C.D. Release of uranium from volcanic glass in sedimentary sequences: An analysis of two systems. *Econ. Geol.* **1981**, *76*, 69–88. [CrossRef]
19. Chen, Z.L.; Liu, J.; Gong, H.L.; Zheng, E.J.; Wang, X.H.; Pan, J.H. Cenozoic tectonic movement and its control on sandstone-type uranium deposits in northern Junggar Basin. *Acta Geol. Sin.* **2006**, *81*, 101–110.
20. Wu, B.L.; Wei, A.J.; Liu, C.Y.; Song, Z.S.; Hu, L.; Wang, D.; Cun, X.N.; Sun, L. Stable isotope tracer of white sandstone in Yan'an Formation in northern Ordos Basin and its geological significance. *Geosci. Front.* **2015**, *22*, 205–214.
21. Hall, S.M.; Mihalasky, M.J.; Tureck, K.R.; Hammarstrom, J.M.; Hannon, M.T. Genetic and grade and tonnage models for sandstone-hosted roll-type uranium deposits, Texas Coastal Plain, USA. *Ore Geol. Rev.* **2017**, *80*, 716–753. [CrossRef]
22. Song, H.; Ni, S.; Chi, G.X.; Zhang, C.J.; Hou, M.C.; Liu, H.X.; Wang, G.; Yan, W.Q. Systematic variations of H-O-C isotopes in different alteration zones of sandstone-hosted uranium deposits in the southern margin of the Yili Basin: A review and implications for the ore-forming mechanisms. *Ore Geol. Rev.* **2019**, *107*, 615–628. [CrossRef]
23. Yue, L. The Formation Process and Evolution Law of Pyrite in Uranium Reservoir in Zhiluo Formation, Northern Ordos Basin. Master's Thesis, China University of Geosciences, Beijing, China, 2021.
24. Jin, R.S.; Miao, P.S.; Sima, X.Z.; Yu, R.A.; Cheng, Y.H.; Tang, C.; Wang, S.Y. Structure styles of Mesozoic–Cenozoic U-bearing rock series in northern China. *Acta Geol. Sin. (Engl. Ed.)* **2016**, *90*, 2104–2116. [CrossRef]
25. Si, Q.H.; Teng, X.M.; Zhu, Q.; Li, J.G.; Zhao, H.L.; Wang, G.M.; Tong, H.K.; Dang, H.L. The origin and migration laws of hydrocarbons in uranium-bearing Luohe Formation, Pengyang area, SW Ordos Basin. *Geol. J.* **2024**, *59*, 2703–2719. [CrossRef]

26. Si, Q.H.; Li, J.G.; Miao, P.S.; Zhang, C.; Zhu, Q.; Zhao, H.L. Characteristics and mechanism of hydrocarbon alteration of faded sandstone in the uranium-bearing Luohe Formation, Pengyang area, southwestern Ordos Basin. *Ore Geol. Rev.* **2021**, *136*, 104500. [CrossRef]
27. Jiao, Y.Q.; Wu, L.Q.; Tao, Z.P.; Yue, L.; Peng, H.; Xiang, Y.; Zhong, W.H.; Li, J.H.; Zhang, C.C.; Bai, W.H.; et al. Metallogenic specificity and prospecting directions of sandstone-type uranium deposits in uranium-bearing series in arid depositional background. *Earth Sci.* **2026**, *51*, 2024–2046.
28. Zhu, Q.; Yu, R.A.; Li, G.Y.; Wen, S.B.; Li, J.G.; Si, Q.H.; Guo, H. Associated mineral assemblages of sandstone-type uranium deposits in the northeastern Ordos Basin and their geological significance. *Geotecton. Metallog.* **2021**, *45*, 327–344.
29. Ding, B.; Liu, H.X.; Xu, D.R.; Qiu, L.F.; Zhang, Z.L.; He, F. Uranium metallogenic effect of hydrothermal fluid transformation in sandstone-type uranium deposits in northern Ordos Basin: Constraints from the study of biotite chloritization process. *Uranium Geol.* **2024**, *40*, 125–134.
30. Yang, T.X.; Yu, R.A.; Rong, H.; Li, T.; Zhu, Q.; Si, Q.H.; Tu, J.R.; Peng, S.L. Geochemical characteristics of Middle Jurassic Zhiluo Formation and its implications for uranium mineralization in northeastern Ordos Basin. *North China Geol.* **2023**, *46*, 35–46.
31. Liu, C.Y.; Zhao, H.G.; Wang, F.; Chen, H. Attributes of the Mesozoic structure on the west margin of the Ordos Basin. *Acta Geol. Sin.* **2005**, *79*, 737–747.
32. Zou, S.; He, D.F.; Cheng, X.; Mao, D.F. Analysis of regional structural cross section in the northern section of the western edge of the Ordos Basin and new insights into Qipanjing syncline structure. *Chin. J. Geol.* **2024**, *59*, 712–722.
33. Zhu, Q.; Wu, Y.; Wen, S.B.; Wang, Y.; Li, G.Y.; Si, Q.H.; Zhao, H.L. Analysis and comparative research on metallogenic geological characteristics of sandstone-type uranium deposits between Zhiluo Formation and Luohe Formation in Ordos Basin. *North China Geol.* **2022**, *45*, 28–37.
34. Sun, X.; Li, L.; Ding, C. Unconformity structure types and hydrocarbon migration characteristics in Hangjinqi area, Ordos Basin. *Oil Gas. Geol.* **2016**, *37*, 165–172.
35. Chen, L.L.; Jin, R.S.; Zhao, H.L. The characteristics of sedimentary system of lower Cretaceous Luohe Formation in Pengyang uranium deposit hosted by aeolian sandstone, southwestern Ordos basin, China: Implications for uranium mineralization. *Geol. Ore Depos.* **2025**, *67*, 504–527. [CrossRef]
36. Gromet, L.P.; Haskin, L.A.; Korotev, R.L.; Dymek, R.F. The "North American shale composite": Its compilation, major and trace element characteristics. *Geochim. Cosmochim. Acta* **1984**, *48*, 2469–2482. [CrossRef]
37. Bodnar, R.J. Revised equation and table for determining the freezing point depression of H_2O–NaCl solutions. *Geochim. Cosmochim. Acta* **1993**, *57*, 683–684. [CrossRef]
38. Langmuir, D. Uranium solution-mineral equilibria at low temperatures with applications to sedimentary ore deposits. *Geochim. Cosmochim. Acta* **1978**, *42*, 547–569. [CrossRef]
39. Zhang, L.; Liu, C.Y.; Zhao, Z.P. Fluid action and mineralization of sandstone-type uranium deposits in Hangjinqi area, Ordos Basin. *Earth Sci. Front.* **2015**, *22*, 368–381.
40. Xu, H.Y. Study on Mesozoic Structural Characteristics and Tectonic Evolution in Hangjinqi Area, Northern Ordos Basin. Master's Thesis, China University of Petroleum (Beijing), Beijing, China, 2018.
41. Szenknect, S.; Alby, D.; López García, M.; Wang, C.; Podor, R.; Miserque, F.; Mesbah, A.; Duro, L.; Zetterström Evins, L.; Dacheux, N.; et al. Coffinite formation from UO_{2+x}. *Sci. Rep.* **2020**, *10*, 11677. [CrossRef] [PubMed]
42. Wersin, P.; Hochella, M.F.; Persson, P.; Redden, G.; Leckie, J.O.; Harris, D.W. Interaction between aqueous uranium (VI) and sulfide minerals: Spectroscopic evidence for sorption and reduction. *Geochim. Cosmochim. Acta* **1994**, *58*, 2829–2843. [CrossRef]
43. Tian, J.F.; Yu, J.; Zhang, Z.G. Research progress on alkaline dissolution in sandstones. *Bull. Geol. Sci. Technol.* **2022**, *41*, 83–93,100.
44. Luo, X.J.; Yang, W.D.; Li, R.X.; Gao, L.P. Effect of pH on feldspar solubility and secondary porosity development. *Bull. Mineral. Petrol. Geochem.* **2001**, *2*, 103–107.
45. Zhang, S.H.; Zhao, Y.; Liu, J.M.; Hu, J.M.; Song, B.; Liu, J.; Wu, H. Geochronology, geochemistry and tectonic setting of the Late Paleozoic–Early Mesozoic magmatism in the northern margin of the North China Block: A preliminary review. *Acta Petrol. Mineral.* **2010**, *29*, 824–842.
46. Yang, T.X.; Yu, R.A.; Rong, H.; Li, T.; Zhu, Q.; Si, Q.H.; Tu, J.R.; Peng, S.L. Geochemistry of sandstones and U-Pb ages of detrital zircons in the Zhiluo Formation of the central and northern Ordos Basin, China: Constraints on provenance and tectonic setting. *Acta Geosci. Sin.* **2024**, *45*, 941–952.
47. Cai, C.F.; Li, H.T.; Qin, M.K.; Luo, X.R.; Wang, F.Y.; Ou, G.X. Biogenic and petroleum-related ore-forming processes in Dongsheng uranium deposit, NW China. *Ore Geol. Rev.* **2007**, *32*, 262–274. [CrossRef]
48. Feng, X.X.; Jin, R.S.; Sima, X.Z.; Li, J.G.; Zhao, H.L.; Chen, Y.; Chen, L.L.; Tang, C.; Ao, C.; Wang, X.H. Uranium-source tracing of the Dongsheng uranium ore field, Ordos Basin and its geological significance. *Geol. China* **2017**, *44*, 623–639.
49. Zhu, Q.; Yu, R.A.; Li, J.G.; Sima, X.Z.; Si, Q.H.; Li, G.Y.; Wen, S.B.; Liu, X.X.; Wang, S.B. Control of reducing media on sandstone-type uranium deposits in Tarangaole area, northeastern Ordos Basin. *Coal Geol. Explor.* **2018**, *46*, 112–118.

50. Geng, H.B.; Shi, M.C.; Fu, S.Q.; An, L.P. Simulation study of mineralization of sulfate-reducing bacteria in Dongsheng sandstone-type uranium deposit. *Acta Sedimentol. Sin.* **2021**, *39*, 886–893.
51. Zhang, L.J.; An, S.Q.; Xu, T.M.; Zhang, N.; Wei, S.; Fang, P.D. Study on influencing factors for reduction capacity of gray-green sandstone in Ordos sandstone-type uranium deposits. *Rock Mineral. Anal.* **2018**, *37*, 396–403.
52. Wen, S.B.; Zhu, Q.; Cheng, Y.H. Occurrence characteristics of ore bodies in the Tarangaole uranium deposit, Ordos Basin and their indication for mineralization. *North China Geol.* **2025**, *48*, 32–42.
53. Li, T.; Yu, R.A.; Rong, H.; Yang, T.X.; Si, Q.H.; Zhu, Q.; Peng, S.L.; Tang, Y.X.; Quan, X.Q. Geological characteristics and metallogenic analysis of sandstone-type uranium deposits in Baiyanhua area, western Erlian Basin, Inner Mongolia. *Geol. China* **2025**, *52*, 1823–1839.
54. Zhu, Q.; Si, Q.H.; Wen, S.B.; Yu, R.A.; Li, G.Y.; Zhang, B.; Wang, S.B.; Peng, S.L.; Li, J.M. Petrological-mineralogical characteristics of Saihan Formation in Sanggendala Sag, Erlian Basin and their implications for uranium enrichment. *Acta Geosci. Sin.* **2026**, *47*, 805–819.
55. Feng, Z.B.; She, S.Y.; Bai, L.; Zhang, X.; Li, L.Y.; Jiang, L.; Qi, Z.S.; Shi, J.L.; Wang, X.F. Research status and development trend of sandstone-type uranium deposit metallogenic structures in China. *North China Geol.* **2025**, *48*, 1–16.
56. Ding, B.; Liu, H.X.; Qiu, L.F.; Zhang, Z.L.; Xu, D.R. Ilmenite alteration and its adsorption and catalytic reduction in U enrichment in sandstone-hosted U deposits from the northern Ordos Basin, North China. *Minerals* **2022**, *12*, 167. [CrossRef]
57. Hua, B.; Xu, H.; Terry, J.; Deng, B. Kinetics of uranium (VI) reduction by hydrogen sulfide in anoxic aqueous systems. *Environ. Sci. Technol.* **2006**, *40*, 4666–4671. [CrossRef] [PubMed]
58. Wan, J.; Tokunaga, T.K.; Kim, Y.; Brodie, E.L. Uranium (IV) adsorption by natural organic matter in anoxic sediments. *Proc. Natl. Acad. Sci. USA* **2017**, *114*, 711–716. [CrossRef] [PubMed]

Disclaimer/Publisher's Note: The statements, opinions and data contained in all publications are solely those of the individual author(s) and contributor(s) and not of MDPI and/or the editor(s). MDPI and/or the editor(s) disclaim responsibility for any injury to people or property resulting from any ideas, methods, instructions or products referred to in the content.